Electronic Supplementary Material (ESI) for Journal of Materials Chemistry A.

Supplemental Information

Comparison of Bladed and Spun Films

Films prepared via spin-coating and doctor blading were compared directly to each other to ensure the compatibility of the results. The spun films were prepared using a well-established literature recipe[11, 14, 15, 21, 26, 35], 21 mg/mL *p*-DTS(FBTTh$_2$)$_2$ and 14 g/mL [70]PCBM were co-dissolved at 90 °C in chlorobenzene solution resulting in 35 mg/mL total content of *p*-DTS(FBTTh$_2$)$_2$ and PCBM. Prior usage the hot solution was filtered through a 0.45 um PTFE filter into a 70 °C warm mininert vial. Additionally to the neat small molecule / fullerene solution, a second solution with the addition of 0.4 % volume fraction 1,8-diiodooctane (DIO) was prepared, which has been shown to be the optimum amount for this system yielding power conversion efficiencies (PCEs) above 7 %.[11, 26, 35] Films for X-ray diffraction measurements were spun on PEDOT:PSS coated silicon substrates to match films prepared in the solar cell configuration. Blade coated films were prepared in a similar manner, except the mass concentration of p-DTS(FBTTh$_2$)$_2$ and [70]PCBM in solution was increased. To ensure a comparable film thickness, 36mg/ml *p*-DTS(FBTTh$_2$)$_2$ and 24mg/ml [70]PCBM were dissolved (60 mg/mL total). To account for the higher small molecule concentration in solution the amount of DIO was increased to 0.6% DIO.

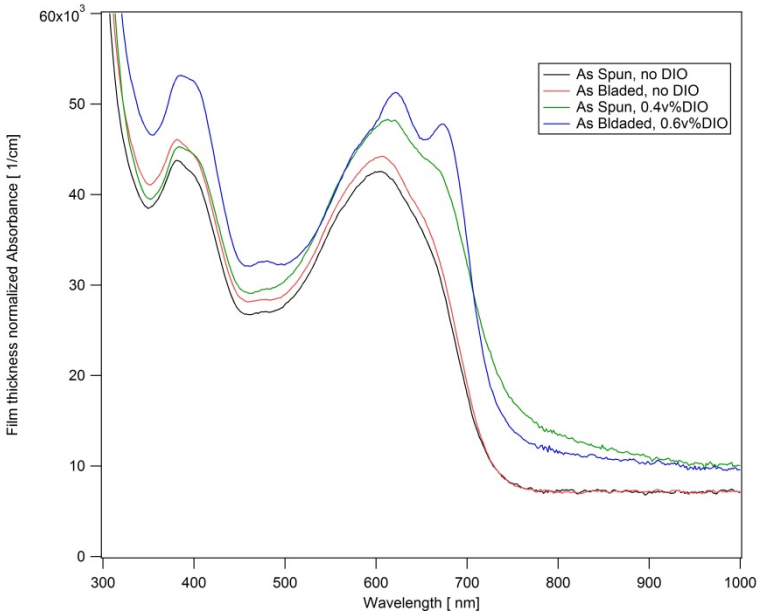

Figure S1 - Absorbance spectra of bladed and spun coated *p*-DTS(FBTTh$_2$)$_2$:[70]PCBM BHJs coated on glass substrates. The absorbance was normalized with respect to the film thickness of the films. Both additive-free spectra significantly lack the presence of the high wavelength shoulder attributed to crystalline order. The additive containing films exhibit characteristics of enhanced crystallinity

	Spun	Bladed
Neat	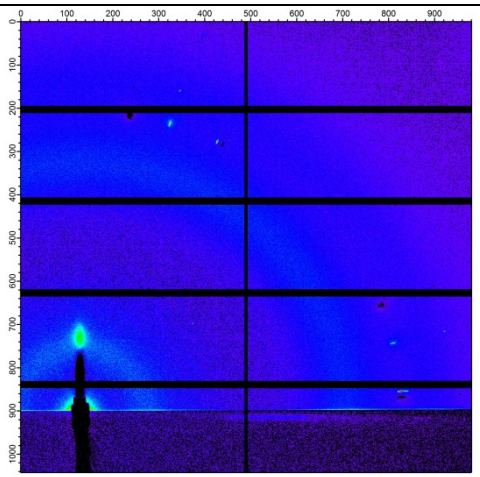	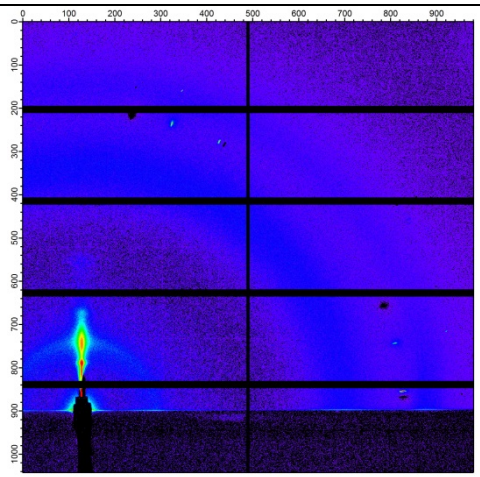
+ DIO	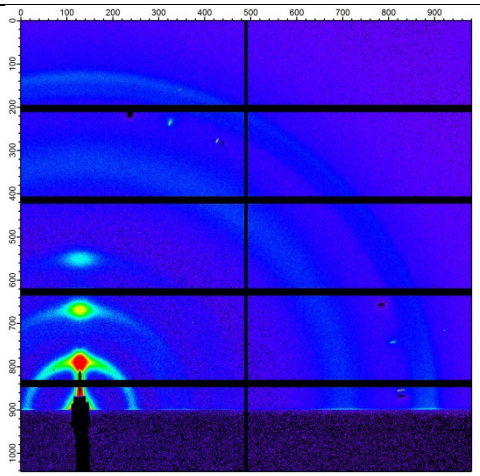	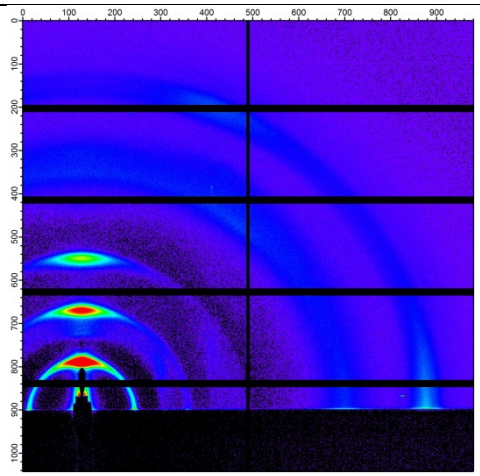

Figure S2 - Background corrected 2D-GIWAXS diffraction pattern of dry *p*-DTS(FBTTh$_2$)$_2$: [70]PCBM films. Spun films are shown on the left, their bladed counterparts on the right. Top: Films cast without processing additive, bottom: films spun (bladed) with addition of 0.4 % (0.6 %) DIO. For all images, the signal is presented on a logarithmic scale and same colour map was used.

Figure S2 shows the background and film thickness corrected 2D-GIWAXS diffraction patterns. The addition of only a small volume percentage of DIO leads to massively enhanced crystallinity. The circular averaged data (over all polar angles azimuthally integrated intensity, shown in Figure S3) further reveals the presence of two different polymorphs in the DIO containing films. On the other hand, as cast glassy films without the additive show none of the two polymorphs and instead show a broad peak at scattering vector q slightly below 0.4 Å^{-1}. These observations are in very good agreement with previously reported data.[21, 26]

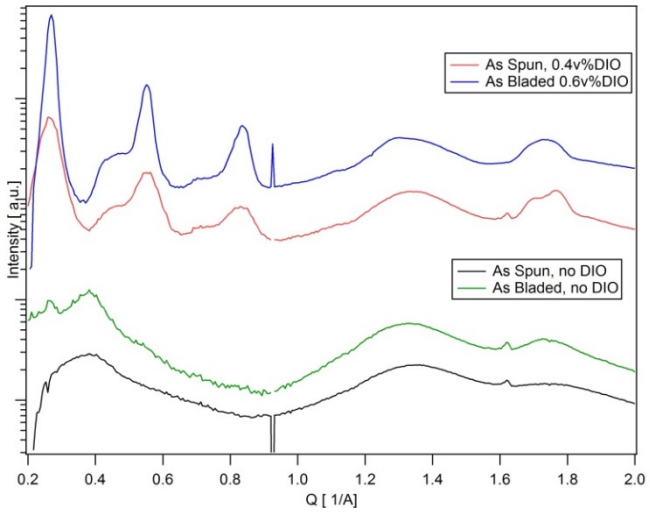

Figure S3 - Circular averages of the 2D-GIWAXS diffraction patterns for dry *p*-DTS(FBTTh$_2$)$_2$: [70]PCBM films. Compared are films cast via spin-coating versus their counterparts cast by doctor blading. No additional processing step after casting was performed. For the ease of comparison the diffraction patterns are translated vertically.

Polymorphs

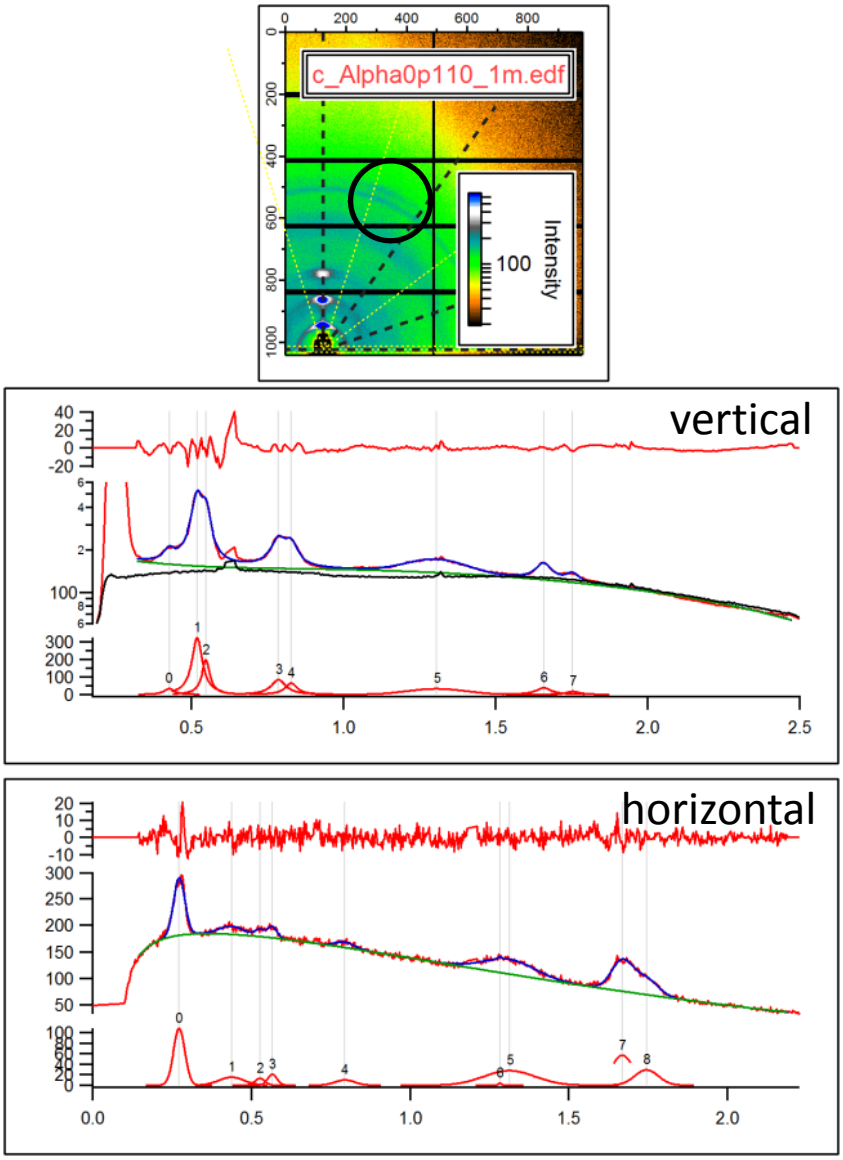

Figure S4 - Shown on top is a high fidelity GIXD image for the 0.6 % DIO case. Indicated are vertical and horizontal line cuts. The extracted line profiles are shown in the two graphs below the detector image, as well as fits to a number of Gaussian peaks and the residuum. The (00l) series can clearly be resolved into two components, summarized in table S1. The (141) feature attributed to pi-pi ordering also exhibits 2 components, but the relationship between them (* and **) and the two (00l) series is not clear.

Table S1: Peak position of the (00l) series and (141) peaks. The data was extracted from the vertical and horizontal line cuts shown in Figure S4. The uncertainty in the given positions is 0.02 $Å^{-1}$, which are the combined uncertainties of the fit and the uncertainty in the determination of the position of the sample horizon.

Assignment	Vertical [$Å^{-1}$]	Horizontal [$Å^{-1}$]
001 (a)	0.25	
001 (b)	0.27	0.27
Metastable phase	0.43	0.44
002 (a)	0.52	0.53
002 (b)	0.55	0.55
003 (a)	0.79	
003 (b)	0.83	
[70]PCBM	1.31	1.31
141 (*)	1.66	1.67
141 (**)	1.75	1.75

Pole Figures - Orientation Factor

Assuming cylindrical symmetry around the sample normal, the corrected intensity equals *I(ω)*sin(ω),* with ω being the pole angle. The integral is then a relative measure for the crystal volume of the corresponding polymorph. We want to point out that due to the difference in the dominant crystalline structure in early times, the total crystal volume is not equal to the volume of the 0.27Å^{-1} structure. Additionally to the integral of the corrected pole figure the Hermann's orientation factor, defined as

$$\langle P_2 \rangle = \frac{\int_0^{90} I(\omega)\sin(\omega)\cdot P_2\, d\omega}{\int_0^{90} I(\omega)\sin(\omega)\, d\omega} \langle P_2 \rangle = \frac{\int_0^{90} I(\omega)\sin(\omega)\cdot P_2}{\int_0^{90} I(\omega)\sin(\omega)} \quad \text{with} \quad P_2 = \frac{3}{2}cos^2(\omega) - \frac{1}{2}\, P_2 = \frac{1}{2}(3cos^2\omega - 1)$$

is given. The orientation factor of an isotropic sample will equal zero, while taking unity for preferential orientation parallel to the sample normal and minus 1/2 for perpendicular orientation for the feature of interest. The initial film orientation is slightly edge on. In the case of both the 0.6 % and 1.0 % volume fraction solutions, the average film orientation becomes more isotropic at long times. In the case of the 1.0 % volume fraction film, the final pole figure appears bimodal with a distinct face-on component.

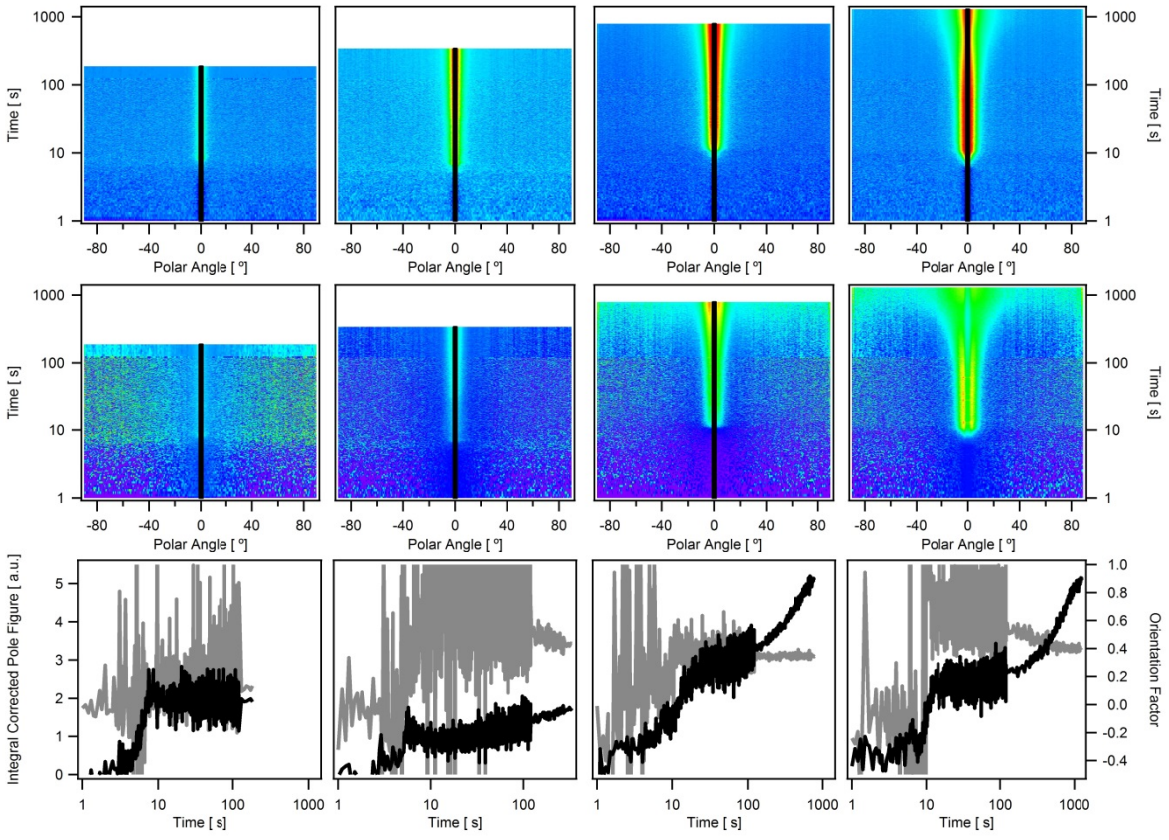

Figure S5 - Time series of the (001) pole figure: raw data (Top), corrected (Middle). Integrate value of the corrected pole figure (black) and Hermann's orientation factor (grey) as extracted from the time series (Bottom). The orientation factor equals 1 for perfect edge-on orientation of the (100), 0 for an isotropic sample and -0.5 for all face-on orientation. The additive amount is increasing from left to right from 0.0 % to 1 % DIO in solution.

Thermal expansion measurements – Glass transition temperature T_g

We monitored the film thickness of both a pristine small molecule film and a BHJ on silicon substrates in the temperature range between room temperature and 160 °C. The heating rate was 5 °C /min. The film thickness was in-situ determined via spectroscopic ellipsometry, fitting the ellipsometric data psi and delta below the optical bandgap to an optical model consisting of the film of interested, represented by a Cauchy model, on top of silicon with natural oxide. Figure S5 shows the film thickness vs. temperature.

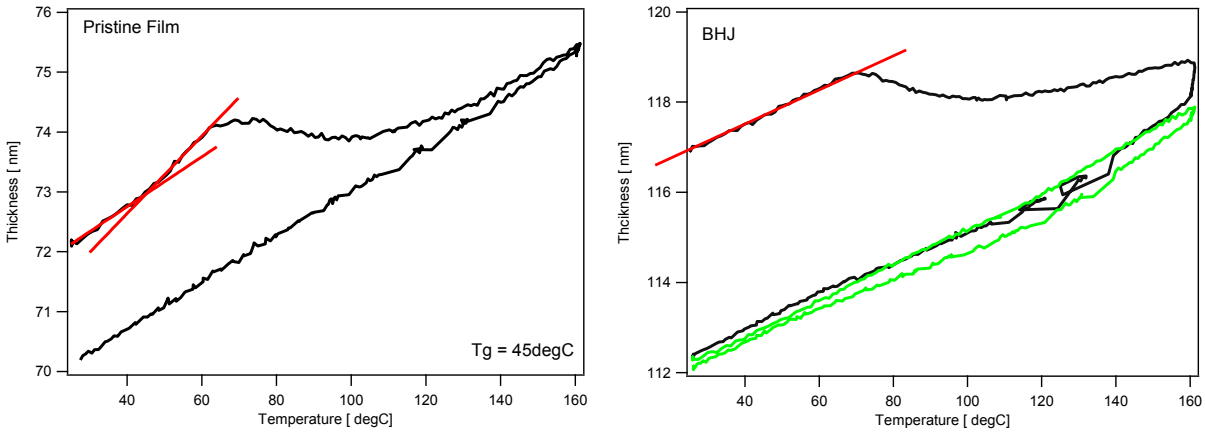

Figure S6 - Film thickness as function of temperature. Pristine small molecule (left) and BHJ film (right) on silicon. The first thermo-cycle is shown in black, the second in green. Red lines indicate the region of linear thermal expansion.

We estimate the T_g of the pristine small molecule from the intersection of the linear thermal expansion regions, indicated in the graph above, to be around (45 ± 10) °C, in the case of the BHJ the T_g could not be measured due to a simultaneously occurring cold crystallization / structure transition of the metastable polymorph between 70 °C and 110 °C. The onset of the cold crystallization coincidences with reported annealing temperatures for optimized solar cells in cases where DIO was used as processing additive[11, 21, 26]. We have recently estimated the T_g of [70]PCBM to be ≈ (160 ± 10) °C. Thus simple mixing rules will place T_g of the amorphous mixed glass well above 40 °C.

GISAXS 2D Detector Images at the end of the film drying & TEM

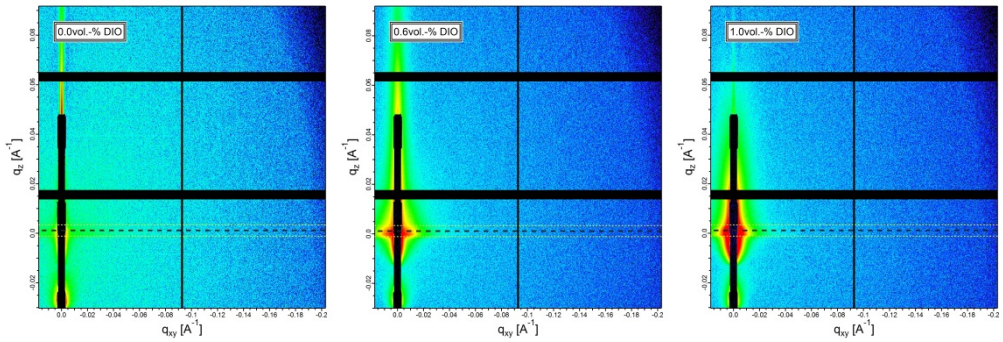

Figure S7: GISAXS detector images of the dry films in case of additive-free, 0.6 % and 1.0 % additive. The Kratky plots reported in Figure 4 of the main manuscript were taken near the sample horizon and is indicated in the images above.

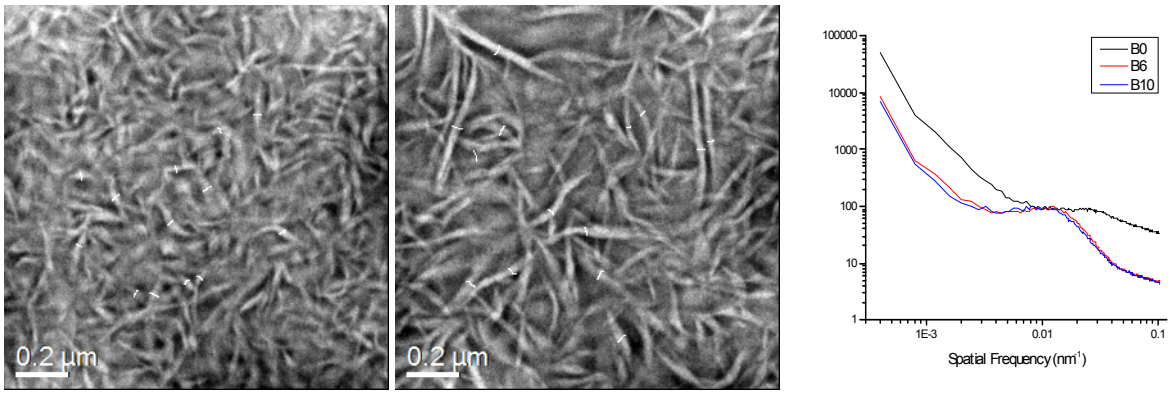

Figure S8: TEM images as reported in Fig 4. The aaverage fiber width is (33 ± 7) nm (left image) and (34 ± 7) nm (center). Right radially averaged FFT data of the three films reported in the main manuscript (neat BHJ without additive – B0, with 0.6% DIO – B6 and 1% DIO – B100). The hump in the two additive cases corresponds to a spatial frequency of about 0.012 nm^{-1} (52 nm).

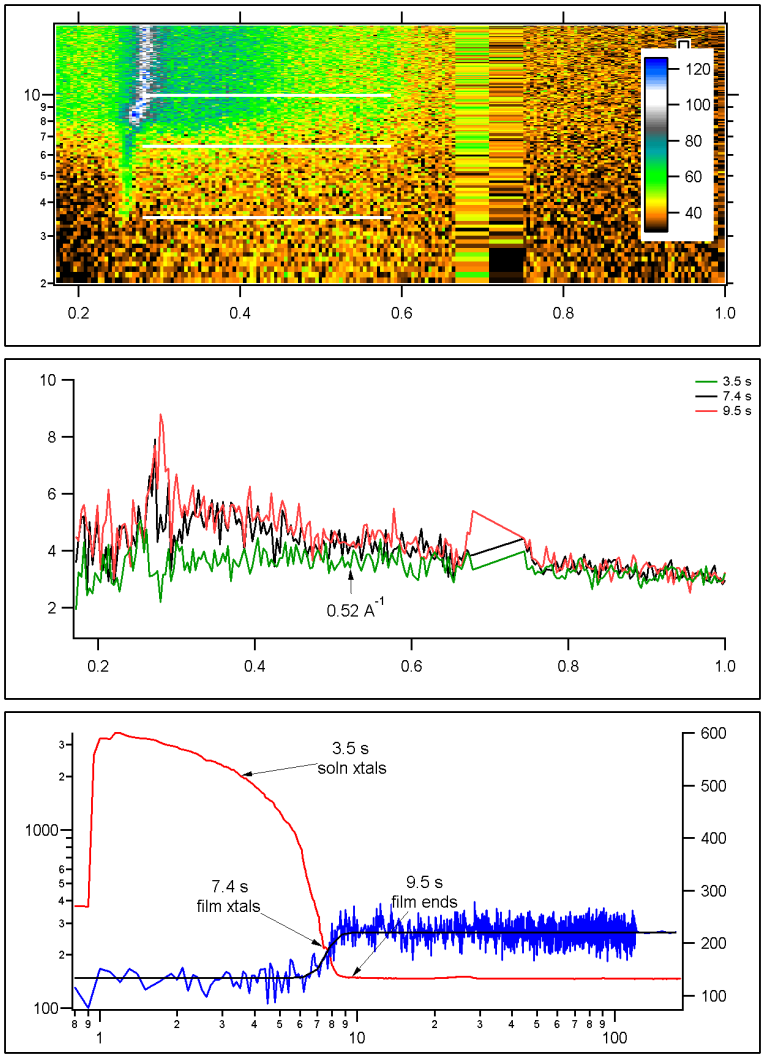

Figure S9: SA detail of early time behaviour of additive-free BHJ. Onset of solution crystallization (0.25 Å^{-1}), film crystallization (0.36 Å^{-1}), and end of film evolution determined "by eye". Pole figure determined by integral from (0.21 to 0.52) Å^{-1}.

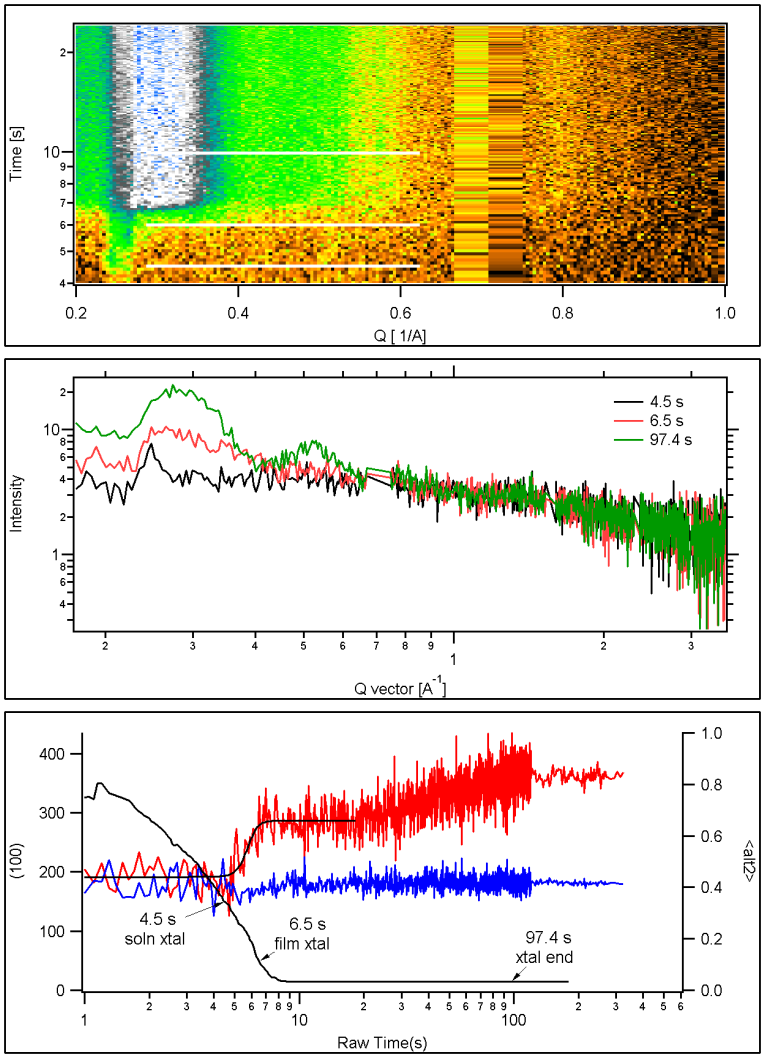

Figure S10: Detail of early time behaviour of additive volume fraction 0.3 % BHJ. Onset of solution crystallization (0.25 $Å^{-1}$), film crystallization (0.36 $Å^{-1}$), and end of film evolution determined "by eye". Pole figure determined by integral from (0.21 to 0.43) $Å^{-1}$.

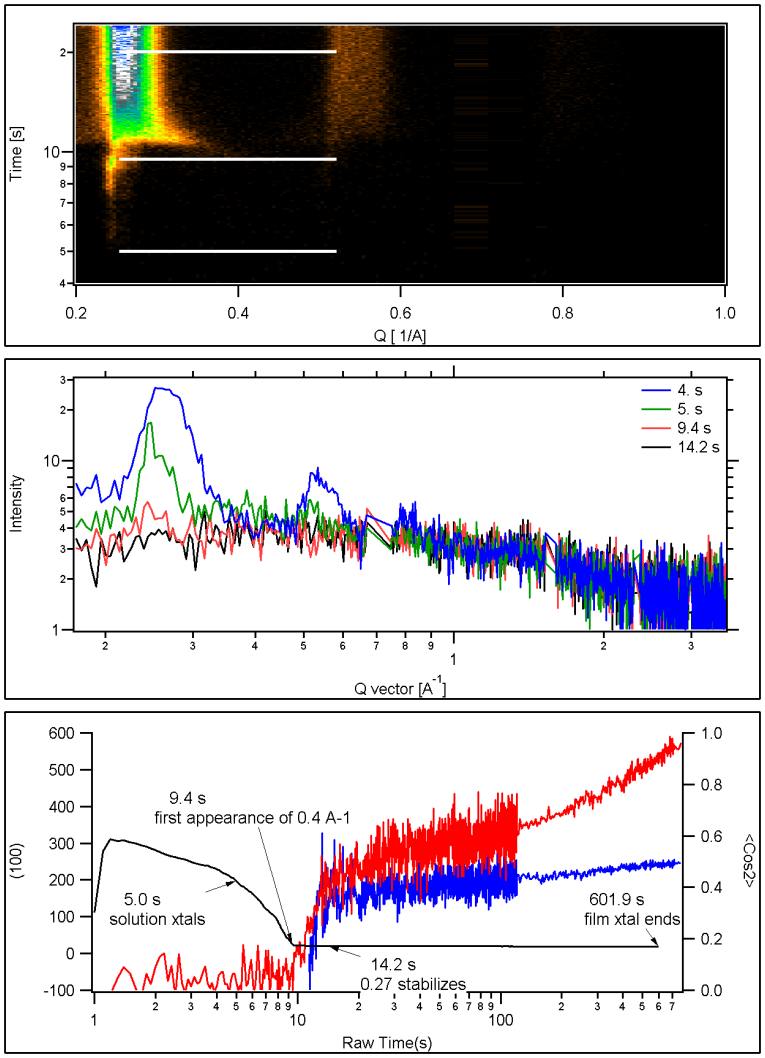

Figure S11: Detail of early time behaviour of additive volume fraction 0.6 % BHJ. Onset of solution crystallization (0.25 $Å^{-1}$), film crystallization (0.36 $Å^{-1}$), and end of film evolution determined "by eye". Pole figure determined by integral from (0.21 to 0.33) $Å^{-1}$.

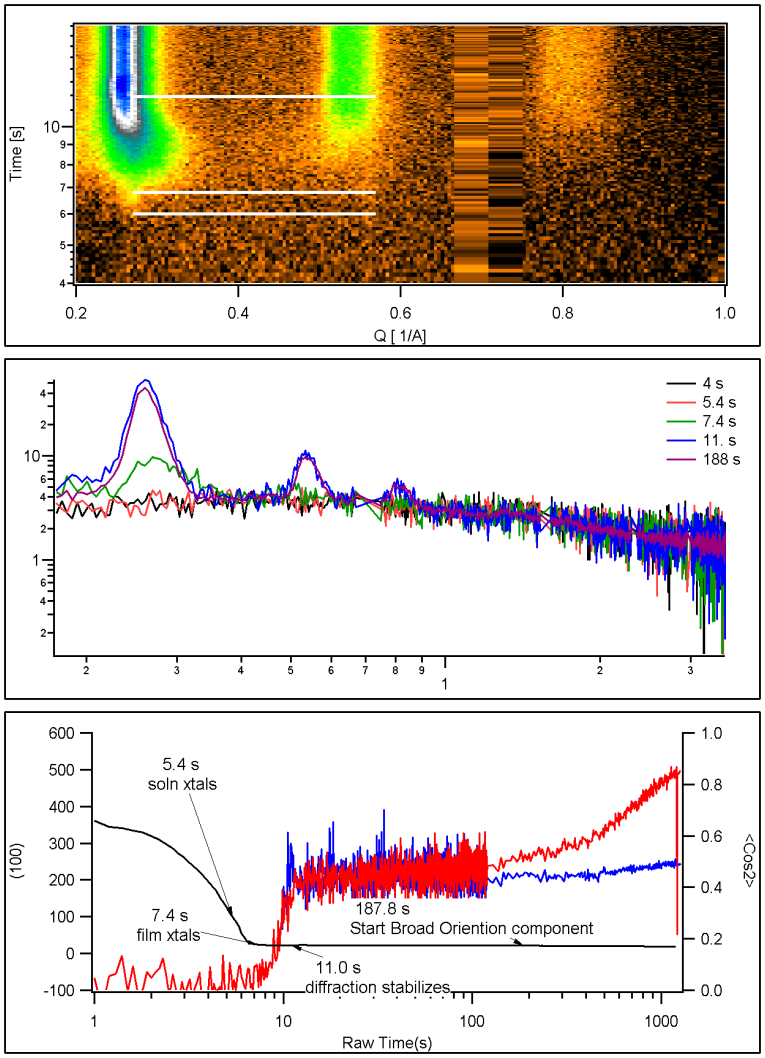

Figure S12: Detail of early time behaviour of additive volume fraction 1.0 % BHJ. Onset of solution crystallization (0.25 $Å^{-1}$), film crystallization (0.36 $Å^{-1}$), and end of film evolution determined "by eye". Pole figure determined by integral from (0.21 to 0.33) $Å^{-1}$

Temperature Dependent Solubility of p-DTS(FBTTh2)2 in Chlorobenzene

The solubility of p-DTS(FBTTh$_2$)$_2$ in the main solvent chlorobenzene was determined via the evaluation of solution UV-Vis data. A reference solution 2.65 mg/ml was prepared by dissolving 5.32mg of p-DTS(FBTTh$_2$)$_2$ in 2ml CB overnight. This solution was then further diluted to 0.177 mg/ml, 0.126 mg/ml and 0.065 mg/ml. For each of those, transmission spectra were taken for 5 optical path lengths between 100 and 500um. The peak amplitude of the main absorption feature around 590nm was extracted and plotted versus the optical path length to extract the molar extinction coefficient ε(9.84E7 +- 2E5) cm^2/mol.
To determine the temperature dependent solubility of the material a solution of nominally 105 mg/ml in CB was prepared. The solution was heated to 80degC and stirred overnight. Prior to use the solution was filtered "hot" through a 0.45um PTFE filter. The glass syringe and the vial receiving the highly concentrated solution were preheated to 80degC. From the filtered solution 5um were added to 2000ul of CB. This solution was again measured via UV-Vis at 5 different

optical path lengths. Using the now known molar extinction of ε = (9.84E7 +- 2E5) cm^2/mol the amount of material after filtering was determined to 99.67mg which is in good agreement with the prepared solution. For the temperature dependent data a small fraction of the undiluted “100 mg/ml” solution was sandwiched between two glass slides preheated to 80degC. The optical path length was set by adhesion forces. Transmission spectra were then taken for controlled temperatures between 80 degC and 30 degC, see Figure S13.

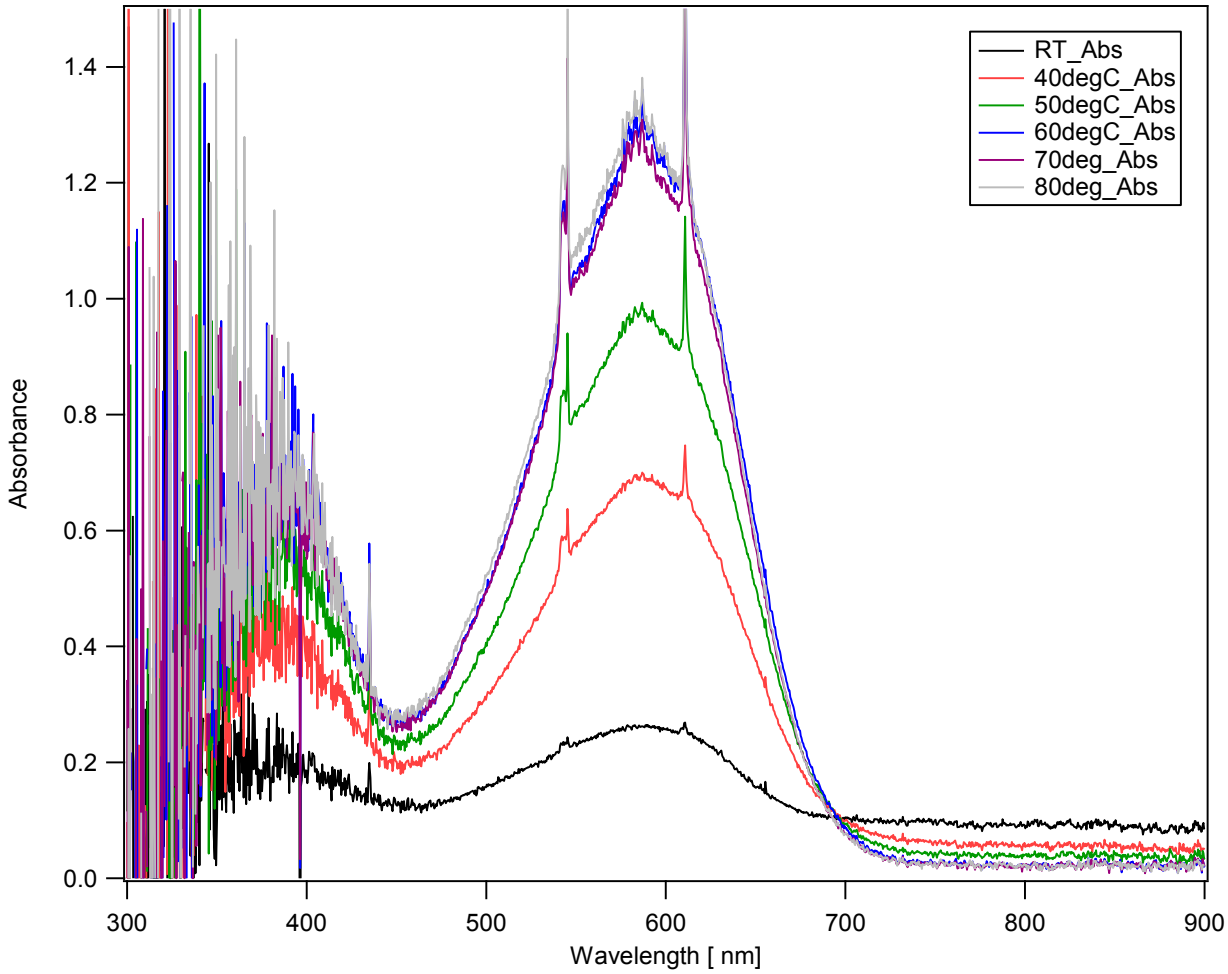

Figure S13: Absorbance spectra of a p-DTS(FBTTh2)2 solution at various temperatures

It is to note that upon cooling no change of the spectral line shape occurs, instead a decrease of absorption around 590nm in combination with an increased scattering fraction (see e.g. long wavelengths) can be observed. We attribute this to the formation of macroscopic p-DTS(FBTTh$_2$)$_2$ crystals which strongly scatter the light. In Figure S14 a microscope image of the near 30degC cold solution is shown. These crystals disappear upon heating to 80degC. From the evaluation of the Absorbance at 590degC and the known concentration we could extract a temperature dependent solubility of p-DTS(FBTTh$_2$)$_2$ in CB, see Figure S15 and Table S2.

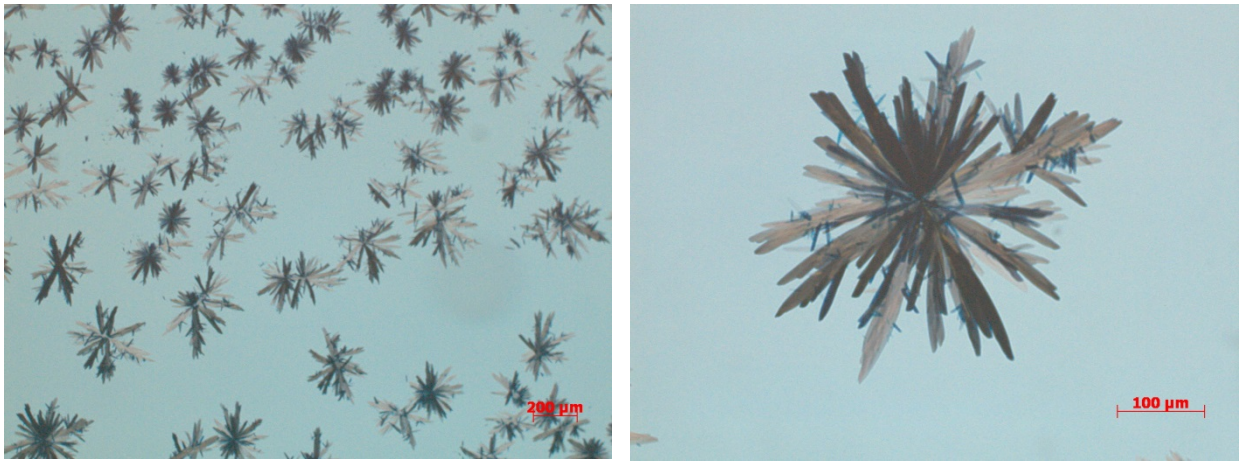

Figure S14: Microscope images of a saturated p-DTS(FBTTh2)2 solution near 30degC. Images taken at 5x (left) and 20x (right) magnification.

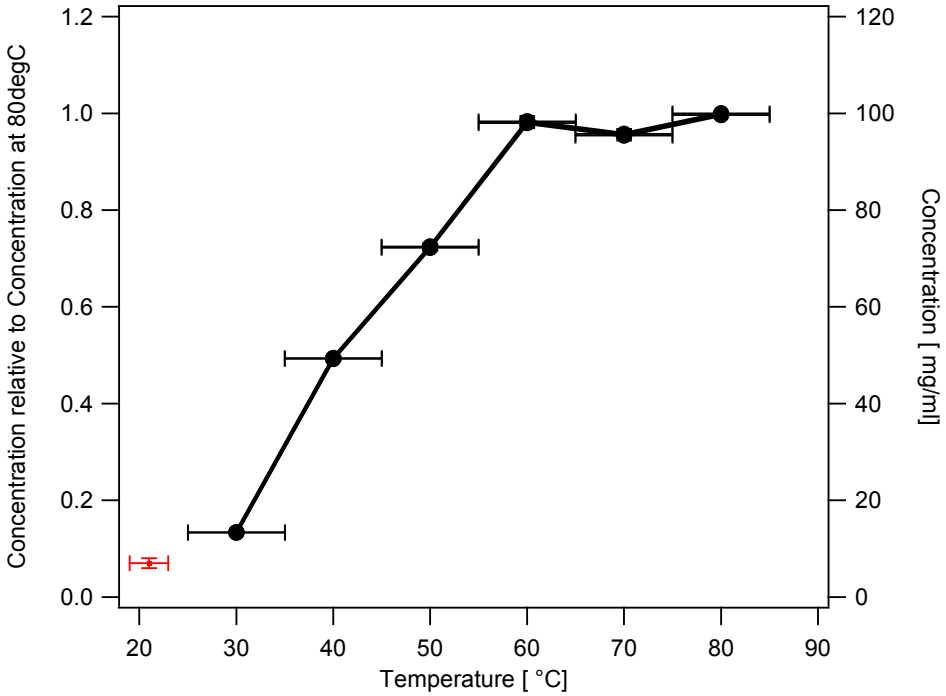

Figure S15: Solubility data for p-DTS(FBTTh2)2 at various temperatures extracted from temperature dependent measurements. The data point is from an independent measurement at room temperature. Please note that above 60degC the concentration limit of the small molecule in CB is not reached and thus reaches a plateau.

Table S2: Solubility of **p-DTS(FBTTh2)2 in chlorobenzene at various temperatures**.

Temperature [degC]	Relative concentration C/C(T=80degC) [rel. u]	Concentration in solution [mg/ml]
30	0.134	13.3
40	0.494	49.2
50	0.725	72.2
60	0.983	98.0
70	0.957	95.4
80	1	99.7